Theoretical Studies on the Structure of Hydration in Perfluorinated Lithium Salt Membranes

Hidekazu Watanabe*,† and Kenta Ooi‡

National Institute of Advanced Industrial Science and Technology, AIST, Hayashi-cho 2217-14, Takamatsu, Kagawa, 761-0395, Japan

Received: January 24, 2005; In Final Form: September 9, 2005

Using an ab initio molecular orbital (MO) method, the normal frequencies are calculated for perfluorinated lithium sulfonate and carboxylate membranes by construction of a cluster model, which severs the ion core from the polymer chain, and then analysis of the experimentally observed infrared (IR) spectra is carried out. During the process of dehydration, small sharp peaks at about 3650 and 3700 cm^{-1} appeared on the shoulder of the broad band at about 3500 cm^{-1}. These sharp peaks are identified as the symmetric and asymmetric stretching modes of the free water molecule. Furthermore, by estimation of the evaporation ratio based on thermochemical analysis, it can be assumed that the first hydration shells are naked in some part of the ion core, thereby allowing evaporation to take place within the external hydration shell during the dehydration process.

1. Introduction

The Nafion membrane, which is the name commonly used for the perfluorinated polymeric sulfonic acids developed by E. I. du Pont Nemours Co., Inc., is an indispensable electrode material for fuel cells. It is well-known that water within the membrane is crucially important for its electrochemical activity. Understanding the function of this water not only is a subject of chemical interest but is also of great importance for advanced applications of these membranes.

The structure of the perfluorinated salt or acid is an ionomer consisting of hydrophobic fluoropolymeric and hydrophilic electrolyte portions, and it is well-known that it has ionic domains.[1] The ionic part is a core with a diameter of 3−10 Å, and the electrolyte and intermediate fluoropolymeric portions are the shell part with a thickness of 3−5 nm around the core part.[2,3] The ionomer membrane contains an appreciable amount of water,[4] which plays an important role in its function. To understand the role of water molecules in the function of the membrane, it is essential to clarify the structure of the water within the membrane, and many studies have attempted to do this using infrared (IR),[5−8] nuclear magnetic resonance (NMR),[9−11] neutron diffraction,[12] and positron annihilation spectroscopy.[13,14] Ostrowska and Narebska found that the infrared spectra changed dramatically, depending upon the water content, however these changes could not be reasonably interpreted.[8] Sondheimer et al. found that the suspension of Nafion particles in acid form is as strongly acidic as CF_3SO_3H.[10] Iwamoto et al. found that the IR spectra change noted on the Nafion membrane which was brought about by dehydration was actually caused by the decomposition of H_3O^+ in equilibrium with RSO_3H and RSO_3^-.[16]

Recently, Iwamoto and co-workers observed the FT-IR spectra for water-contained perfluorinated Li sulfonate membranes (Nafion). Prior to the dehydration process, there was only one broad band at 3512 cm^{-1} in the region of the OH stretching mode of the water molecule. However, two types of adsorption bands have been found by continuously following the dehydration process.[17] The main component has un-separated OH stretching adsorption (νOH) at 3539 cm^{-1}, with two clearly distinct peaks that appear at 3705 and 3640 cm^{-1} as minor components.

Moreover, the IR spectra of the perfluorinated Li carboxylate membranes can also be measured during the process of dehydration. The circumstances surrounding the carboxylate case are very similar to those surrounding the sulfonate case. Only one broad band can be seen prior to the dehydration process, whereas two types of adsorption bands can be observed after dehydration. The main component is a broad band at 3450 cm^{-1} with a shoulder at 3240 cm^{-1}, however a sharp band appears at 3706 cm^{-1} with two shoulders at 3672 and 3643 cm^{-1} as minor components.[17]

In the present paper, we investigate the structure and the normal frequencies for these two kinds of perfluorinated Li salt (sulfonate and carboxylate) membranes which are surrounded by the hydrating water molecules, $RSO_3Li(H_2O)_n$ and $RCO_2Li(H_2O)_n$, using an ab initio molecular orbital (MO) method. All the structures of the perfluorinated Li sulfonate and carboxylate membranes are as follows:

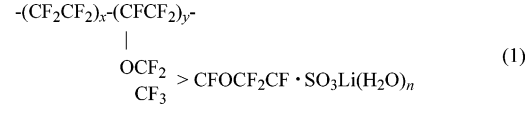

(1)

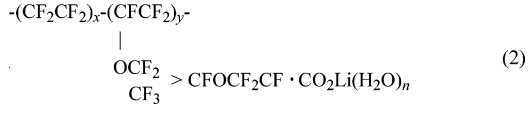

(2)

where both x and y in the main chain are greater than 1.

To perform ab initio MO calculations, the perfluorinated Li salt membranes are clusterized to the side chain together with the ion core consisting of the Li atom and hydrated H_2O molecules that have been cut off from the main chain. The structures of the clusterized perfluorinated side chain with an ion core have been optimized and the normal frequencies have been analyzed.

* Corresponding author. E-mail: hidekazu@cc.kyushu-u.ac.jp.
† Present address: Computing and Communications Center, Kyushu University, Maidashi, 3-1-1, Higashi-ku, Fukuoka, 812-8512, Japan.
‡ Present address: National Institute of Advanced Industrial Science and Technology, AIST, Umezono, 1-1-1, Chuo-2 Tsukuba, 305-8568, Japan.

10.1021/jp050410f CCC: $30.25
Published on Web 10/12/2005

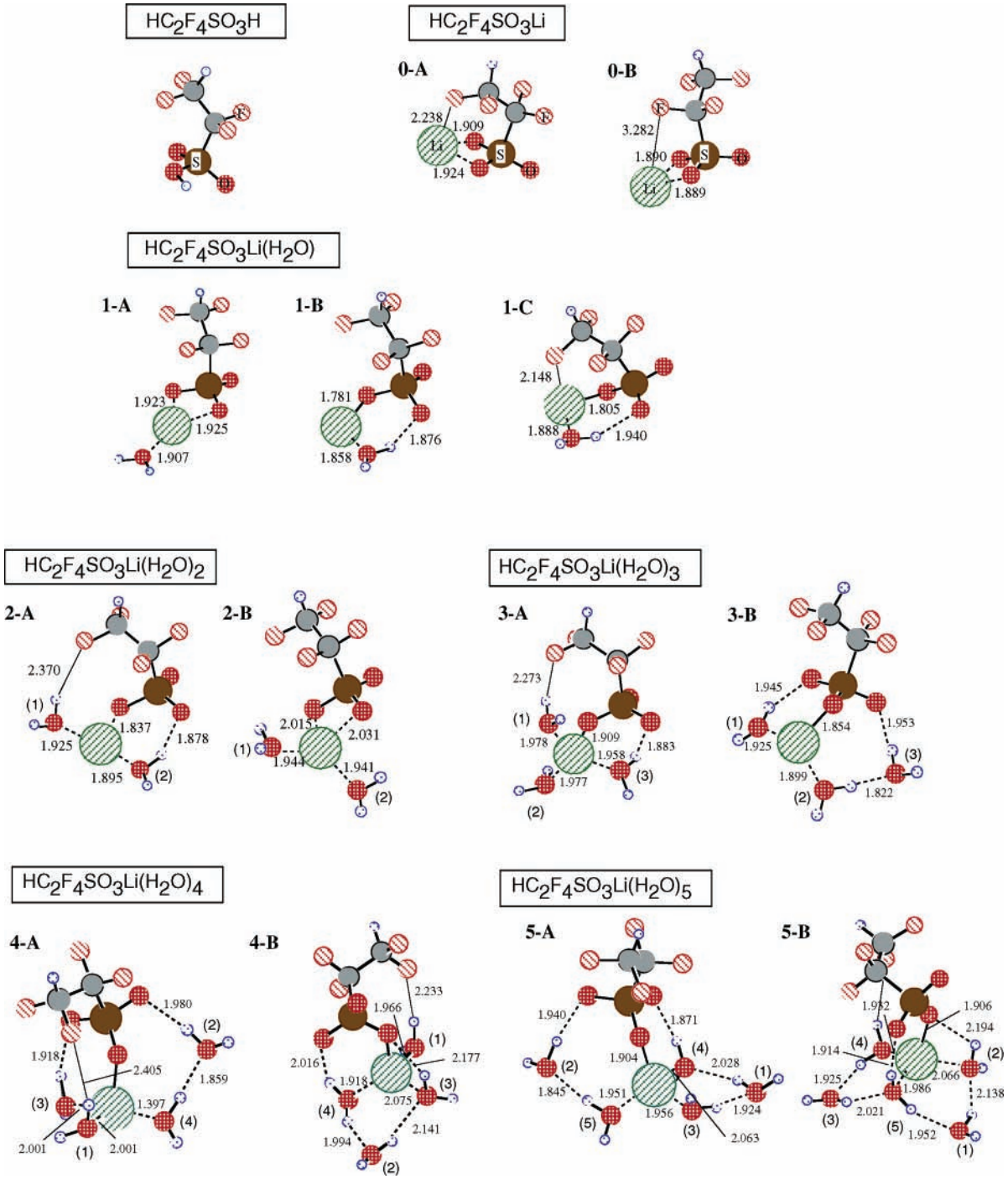

Figure 1. Optimized geometries of the short-chain model for the perfluorinated Li sulfonate membrane $HCF_2CF_2SO_3Li(H_2O)_n$ (up to $n = 5$). The bond lengths are shown in Å calculated with the HF/6-31+G* level on all the atoms. Numbers within round brackets are put for $n \geq 2$ in order to distinguish the H_2O molecules.

2. Methods

Using an ab initio molecular orbital method (MO), the geometric structures were optimized for the clusterized perfluorinated Li salt membranes with the hydrated water molecules, $RSO_3Li(H_2O)_n$ and $RCO_2Li(H_2O)_n$, to analyze the normal frequencies of these membranes. We used two kinds of models: (1) a short-chain model $R = HCF_2CF_2$ and (2) a long-chain model $R = HOCF_2(CF_3)CFOCF_2CF_2$. The long-chain model involves all parts of the perfluorinated side chain. The severed bond is terminated with a hydrogen atom.

In the short-chain model, the 6-31+G* basis set is put on the ionic parts $SO_3Li(H_2O)_n$ and $CO_2Li(H_2O)_n$, while three basis sets, (a) 6-31G, (b) 6-31G*, and (c) 6-31+G*, are put on the HCF_2CF_2 part. Here, the cases of (a) and (b) are denoted as "basis set (a)" and "basis set (b)" respectively. In the case of basis set (c), the 6-31+G* basis set is put on all the atoms. In contrast, in the long-chain model, the 6-31+G* basis set is put on the ion core and CF_2CF_2 part of the side chain, while the 6-31G basis set is put on the remaining part $HOCF_2(CF_3)CFO$. The optimization is carried out at up to $n = 5$ using the short-chain model, and at up to $n = 3$ using the long-chain model. All calculations have been carried out at the Hartree−Fock (HF) level.

At every optimized structure, the harmonic frequencies have been evaluated to confirm the true local minimum. The calculated frequencies have been applied uniformly with a

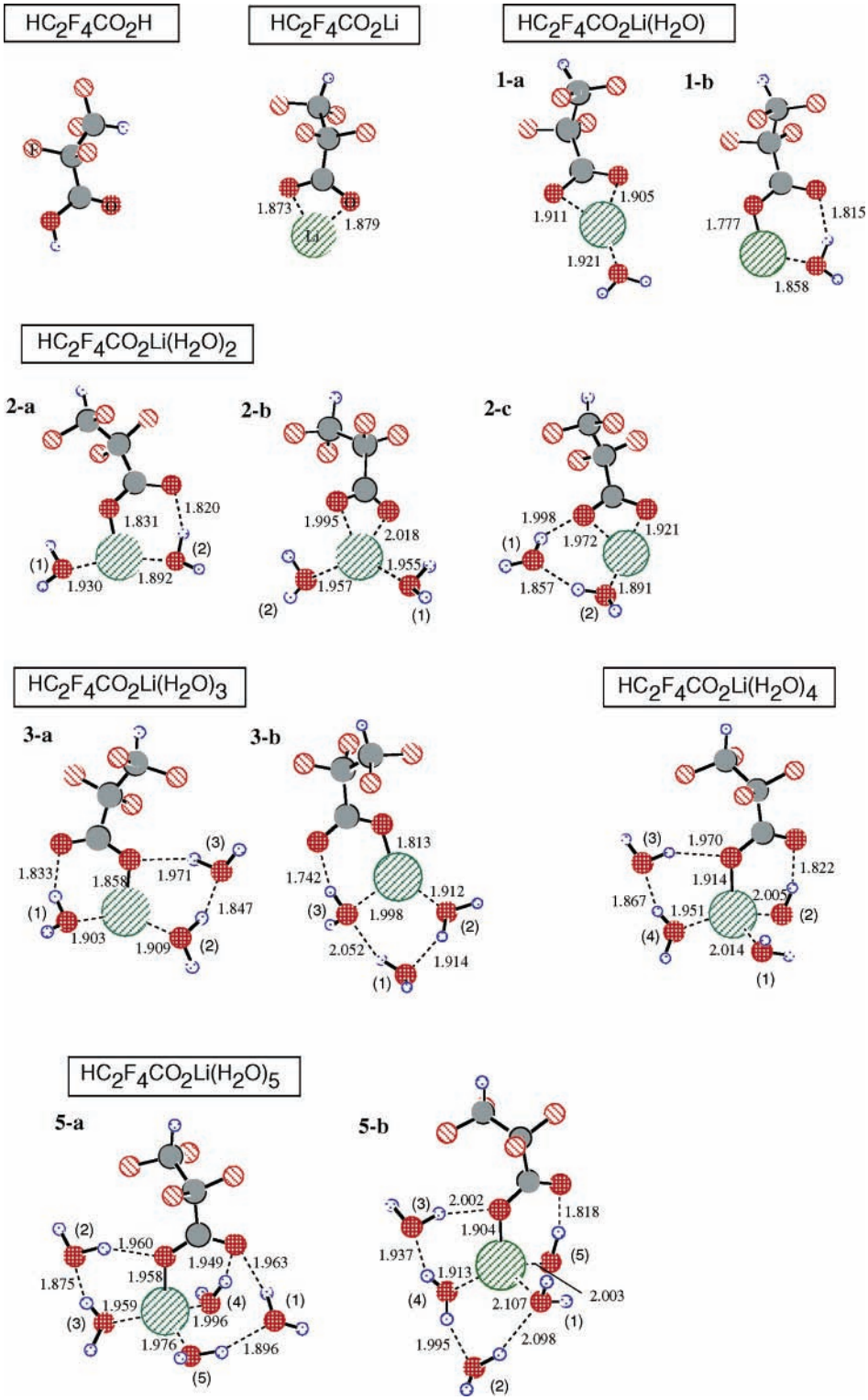

Figure 2. Optimized geometries of the short-chain model for the perfluorinated Li carboxylate membrane $HCF_2CF_2CO_2Li(H_2O)_n$ (up to $n = 5$). The bond lengths are expressed in Å calculated with the HF/6-31+G* level on all the atoms. Numbers within round brackets are put for $n \geq 2$ in order to distinguish the H_2O molecules.

scaling factor of 0.8941 to enable quantitative discussion. The scaling factor was determined with the experimental values of the frequencies of the free water molecule (1595, 3657, and 3756 cm^{-1}). The program used in the ab initio MO calculation is GAUSSIAN 98. [18]

3. Results and Discussion

3.1. Structures. Figures 1 and 2 show the optimized geometries of perfluorinated Li salt membrane systems using the short-chain model $(H(CF_2)_2SO_3Li(H_2O)_n$ and $H(CF_2)_2CO_2Li(H_2O)_n)$. The structural parameters expressed as Å are evaluated with the HF/6-31+G* level on all the atoms. The most stable isomers are labeled with **A** and **a** for each size. The optimized geometries with the long-chain model are shown in Figure 3 for the most stable isomers of $n = 2$ and $n = 3$. The relative energy difference among the isomers (ΔE_{iso}) with zero-point vibration energy (ZPV) correction for all the calculation levels and both cluster models is summarized in Table 1.

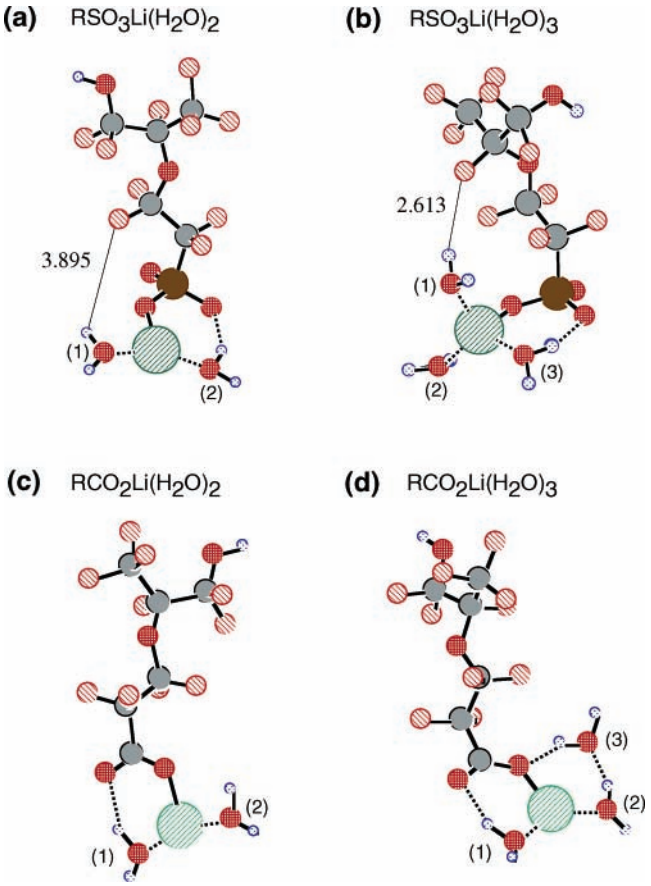

Figure 3. Optimized geometries of the most stable isomers of $RSO_3Li(H_2O)_n$ and $RCO_2Li(H_2O)_n$ for $n = 2$ and $n = 3$ using the long-chain model ($R = HOCF_2(CF_3)CFOCF_2CF_2$). Key: (a) isomer **2-A**; (b) isomer **3-A**; (c) isomer **2-a**; (d) isomer **3-a.** The numbering (1), (2), and (3) for the H_2O molecules is the same as that used in Figures 1 and 2.

TABLE 1: Relative Energy Difference Corrected with the Zero-Point Vibration (ZPV) Energy (ΔE_{Iso}) for the Cluster-Modeled Perfluorinated Lithium Sulfonate and Carboxylate Membranes, $RSO_3Li(H_2O)_n$ and $RCO_2Li(H_2O)_n$

		short-chain			
		basis (a)	basis (b)	HF/6-31+G*	long-chain
$RSO_3Li(H_2O)_n$	**0-A → 0-B**	16.93	7.53	3.42	4.39
	1-A → 1-B	9.73	11.06	10.47	10.35
	1-A → 1-C	3.75	10.83	20.21	*b*
	2-A → 2-B	8.31	3.39	3.15	2.20
	3-A → 3-B	4.73	0.10	0.69	2.13
	4-A → 4-B	28.82	30.49	29.70	
	5-A → 5-B	22.86	25.38	25.51	
$RCO_2Li(H_2O)_n$	**1-a → 1-b**	8.34	7.78	7.12	−1.82
	2-a → 2-b	4.97	6.56	7.48	0.60
	2-a → 2-c	15.06	13.30	15.09	15.58
	3-a → 3-b	21.94	20.90	20.51	10.78
	5-a → 5-b	15.79	16.13	15.41	

[a] Data are expressed as kJ/mol. The basis sets (a) and (b) are used for the 6-31G and the 6-31G* sets on the $H(CF_2)_2$ part, while the 6-31+G* is used on the remaining atoms $SO_3Li(H_2O)_n$ and $CO_2Li(H_2O)_n$. [b] The stationary point does not exist for the isomer **1-C** with the long-chain model.

3.1.1. $n = 0$ and $n = 1$. In the optimized structures for $n = 0$, $H(CF_2)_2SO_3Li$ and $H(CF_2)_2CO_2Li$, neither of which has a hydrated water molecule, the Li atom is bound to two oxygen atoms almost equivalently in the SO_3 and the CO_2 groups, whereas in the structures of $H(CF_2)_2SO_3H$ and $H(CF_2)_2CO_2H$, the H atom is bound to only one of the O atoms, due to the very small atomic radius of the H atom. The most stable structures for $n = 1$ are the isomers **1-A** and **1-a**. The Li atom is bound to two O atoms of the SO_3 and the CO_2 groups in the same way as for $n = 0$. The two O atoms and $LiO-H_2$ form a planar structure. The isomers, **1-B**, **1-C**, and **1-b** are the next stable, and only one O atom of the SO_3 or CO_2 group is directly bound to the Li atom. An additional O atom is bound to the H atom of the H_2O molecule with the hydrogen bond.

We also attempted to search for a stable local minimum structure in which the H atoms of the H_2O molecule are bound to the O atoms of the SO_3 and the CO_2 groups as follows:

$$\text{Li---O} < \begin{matrix} \text{H} \cdots \text{O} \\ \text{H} \cdots \text{O} \end{matrix} > \text{SO-R}, \quad \text{Li---O} < \begin{matrix} \text{H} \cdots \text{O} \\ \text{H} \cdots \text{O} \end{matrix} > \text{C-R} \qquad (3)$$

We found such a reversed isomer for $RCO_2Li(H_2O)_1$ with only the short-chain model, and ΔE_{iso} was located at +162.62 kJ/mol higher than that of the isomer **1-a** with the HF/6-31+G* basis set. In the case of the $RSO_3Li(H_2O)_n$ system, the reversed structure does not have any stationary point. The contribution of the reversed isomer can, therefore, be neglected in both perfluorinated Li salt membrane systems.

3.1.2. $n = 2$ to $n = 5$. The coordination structures of the clusters and the number of hydrogen bonds are summarized in Table 2. The most stable isomers (those labeled with **A** or **a**) for $n \geq 2$ have a structure in which the H_2O molecule is bound to one O atom in the SO_3 or the CO_2 group. With the HF/6-31+G* basis set and short-chain model, the isomers **2-A** and **2-a** are 10.47 and 7.42 kJ/mol more stable than the isomers **2-B** and **2-b**, respectively. Despite $H_2O(1)$ being bound to the O atom of the CO_2 group, the isomer **2-c** is about 15 kJ/mol less stable than the isomer **2-a**, probably due to the distorted sp^2 hybridization orbital of the Li atom caused by the hydrogen bond of $H_2O(1)$ and $H_2O(2)$.

The stability of the $RSO_3Li(H_2O)_3$ cluster is not controlled simply by the number of hydrogen bonds. The isomer **3-A** that

TABLE 2: Coordination Structures of the Isomers Calculated for $HCF_2CF_2SO_3Li(H_2O)_n$ and $HCF_2CF_2CO_2Li(H_2O)_n$ Clusters[a]

		no. of coordinations with Li		no. of hydrogen bonds		
isomers		SO_3-Li or CO_2-Li	H_2O-Li	SO_3-H_2O or CO_2-H_2O	H_2O-H_2O	ΔE_{iso}/kJ mol^{-1}
$RSO_3Li-(H_2O)_n$	**0-A**	2				
	0-B	2				3.42 (**0A → 0B**)
	1-A	2	0	0		
	1-B	1	1	1		10.47 (**1A → 1B**)
	1-C	1	1	1	0	20.21 (**1A → 1C**)
	2-A	1	2	1	0	
	2-B	2	2	0	0	3.15 (**2A → 2B**)
	3-A	1	3	1	0	
	3-B	1	2	2	1	0.69 (**3A → 3B**)
	4-A	1	3	2	1	
	4-B	1	3	2	2	29.70 (**4A → 4B**)
	5-A	1	3	2	3	
	5-B	1	3	2	4	25.51 (**5A → 5B**)
$RCO_2Li-(H_2O)_n$	**0**	2	−	−	−	
	1-a	2	1	0	−	
	1-b	1	1	1	−	7.12 (**1a → 1b**)
	2-a	1	2	1	0	
	2-b	2	2	0	0	7.48 (**2a → 2b**)
	2-c	2	1	1	1	15.09 (**2a → 2c**)
	3-a	1	2	2	1	
	3-b	1	2	1	2	20.51 (**3a → 3b**)
	4	1	3	2	1	
	5-a	1	3	3	2	
	5-b	1	3	2	3	15.41 (**5a → 5b**)

[a] The isomerization energy ΔE_{iso} is calculated with the 6-31+G* basis set by using the short-chain model.

has one H_2O-SO_3 hydrogen bond is more stable than the isomer **3-B** in which there are two H_2O-SO_3 hydrogen bonds. The isomer **3-B** has a structure which is distorted from the planar, and stabilization of the hydrogen bond does not compensate for the destabilization of the distorted structure. The hydrogen bond between H_2O molecules is weaker than the bond of H_2O-SO_3 or H_2O-CO_2. The isomer **3-a** with two CO_2-H_2O hydrogen bonds is about 20 kJ/mol more stable than the isomer **3-b** with one CO_2-H_2O bond plus one H_2O-H_2O bond.

The most stable isomers for $n = 4$ and $n = 5$ for $RSO_3Li(H_2O)_n$ (**4-A** and **5-A**, respectively) have a structure in which the two O atoms in the SO_3 group are bound to the H_2O molecules ($H_2O(2)$ and $H_2O(3)$ in **4-A**, and $H_2O(2)$ and $H_2O(4)$ in **5-A**, respectively.), and all the O atoms of the SO_3 group are bound either to the Li atom or the H_2O molecule. However, in the isomers **4-B** and **5-B**, one O atom of the SO_3 group is free, although the number of hydrogen bonds is equal to or even larger than the isomers **4-A** and **5-A**. In the isomer **5-a**, two H_2O molecules, $H_2O(1)$ and $H_2O(4)$, are bound to the same O atom of the CO_2 group. This structure suggests that the H_2O-CO_2 bond may be strong compared to the H_2O-SO_3 bond.

We can conclude that the most stable state for the larger sizes of *n* has a structure in which all the O atoms of the functional group SO_3 or CO_2 are bound to an Li atom or an H_2O molecule, and that the Li atom has a 4-coordinated structure comprising bonds to the O atom of the functional group and bonds to the H_2O molecules. These results indicate that the hydrogen bonds of H_2O-SO_3 and H_2O-CO_2 contribute significantly toward the stabilization, even for clusters with a large hydration number *n*. Furthermore, in $RCO_2Li(H_2O)_n$, we found an isomer in which two H_2O molecules are bound to the same O atom of the CO_2 group. However, priority is expected to be given so that a second hydration shell is constructed when the hydration number *n* is greater than 6, because the space around the O atom of the functional group is occupied by the first hydration shell.

3.2. Description of the Influence of the Perfluorinated Chain. 3.2.1. Interactions within the $RSO_3Li(H_2O)_n$ System. In the $RSO_3Li(H_2O)_n$ system, there are several structures that contain the Li−F bond or the H_2O-F hydrogen bond, and these bonds produce the basis set dependence of the isomerization energy ΔE_{iso} as summarized in Table 1.

The strong basis set dependences of the isomerization energy ΔE_{iso} are observed in **0-A** → **0-B** and **1-A** → **1-C** reactions. The ΔE_{iso} for the reaction **0-A** → **0-B** is 16.93, 7.53, and 3.42 kJ/mol with the basis set (a), basis set (b), and 6-31+G*, respectively, while that for the reaction **1-A** → **1-C** is 3.75, 10.83, and 20.21 kJ/mol, respectively. This can be attributed to the fact that the isomers **0-A** and **1-C** have the Li−F interaction whose strength is overestimated by the small basis set. In contrast, the ΔE_{iso} of **1-A** → **1-B** does not show such a significant basis set dependence, due to the absence of Li−F interaction in the isomers **1-A** and **1-B**.

The H_2O-F hydrogen bond is also overestimated by the basis set (a), however, the basis set (b) provides a good evaluation for the H_2O-F hydrogen bond compared to the 6-31+G* basis set. For example, the ΔE_{iso} of the reaction **2-A** → **2-B** is 8.31, 3.39, and 3.15 kJ/mol with the basis set (a), basis (b), and 6-31+G*, respectively. The ΔE_{iso} with the basis set (b) is very close to that calculated at the HF/6-31+G* level.

On the other hand, the optimized geometry depends on the length of the perfluorinated chain. The Li−F interaction and the H_2O-F hydrogen bond are dissociated with the long-chain model. In the structures of **2-A** and **3-A**, the nearest distances between the H_2O molecule and the F atom ($H_2O(1)-F$) are 2.370 and 2.273 Å with the short-chain model, whereas they are 3.895 and 2.613 Å with the long-chain model, respectively (see also Figure 3 for the long-chain model). Moreover, a stationary point is not found for the isomer **1-C** with the long-chain model.

However, the values of ΔE_{iso} with the long-chain model are very close to those of the short-chain model with the 6-31+G* basis set. The Li−F or $Li-H_2O$ interactions are so weak that they provide only a small contribution toward the stabilization. In the case of the long-chain model, the stabilization energy obtained by these interactions cannot exceed the energy of destabilization due to the entropy reduction caused by the arrangement of the perfluorinated chain.

3.2.2. Interactions within the $RCO_2Li(H_2O)_n$ System. In contrast to the $RSO_3Li(H_2O)_n$ system, the basis set dependence of ΔE_{iso} is not seen in the $RCO_3Li(H_2O)_n$ system because there is no structure involving the Li−F bond and the H_2O-F hydrogen bond. Owing to the planar structure of the CO_2 group, the H_2O molecule and the Li atom may be too far from the perfluorinated chain which produces hydrophobic interaction.

However, the ΔE_{iso} depends on the length of the perfluorinated chain. The isomerization energy **1-a** → **1-b** is 7.12 kJ/mol with the short-chain model (6-31+G*), whereas it is −1.82 kJ/mol with the long-chain model. The isomer **1-b** becomes more stable than the isomer **1-a** with the long-chain model. This may be attributed to the fact that the basicity of the strong base of CO_2 is somewhat weakened by the long perfluorinated chain due to the electron-attracting feature of F atoms, and the strength of the CO_2-Li bonds is overestimated with the short-chain model. Thus, the isomer **1-a** with two CO_2-Li bonds is destabilized when compared to the isomer **1-b** with only one CO_2-Li bond. The CO_2-H_2O bond in the isomer **1-b** may also be overestimated with the short-chain model for the same reason as the CO_2-Li bond. However, the CO_2-H_2O bond is considered to depend less significantly on the chain length than the CO_2-Li bond does.

The isomerization energies (ΔE_{iso}) of the reactions **2-a** → **2-b** and **3-a** → **3-b** are also decreased by about 10 kJ/mol using the long-chain model. Because each of these isomers has one CO_2-Li bond, the decrement of these isomerization energies is attributed to the fact that the strengths of the $CO_2-H_2O(2)$ bond in **2-a** and the $CO_2-H_2O(3)$ bond in **3-a** are weakened due to the decrease in the basicity of CO_2 brought about by the increase in the chain length. Because of the lack of a CO_2-H_2O bond, the isomers **2-b** and **3-b** are relatively stabilized when compared to the isomers **2-a** and **3-a** with the long-chain model. In contrast to these cases, the ΔE_{iso} of the reaction **2-a** → **2-c** does not depend on the chain length, because the isomers **2-a** and **2-c** have the $CO_2-H_2O(2)$ bond.

3.3. Hydration Energy and Gibbs' Function. Figure 4 shows the size dependence of (a) the hydration energy ΔE_{hyd} and (b) the Gibbs function ΔG_{hyd} for the most stable isomers of the perfluorinated Li salt Nafion membrane systems. The hydration reactions of the two membrane systems are defined as

$$RSO_3Li(H_2O)_{n-1} + H_2O \rightarrow RSO_3Li(H_2O)_n \qquad (4)$$

and

$$RCO_2Li(H_2O)_{n-1} + H_2O \rightarrow RCO_2Li(H_2O)_n \qquad (5)$$

For each size of *n*, the most stable isomers **1-A**, **2-A**, ..., and **1-a**, **2-a**, ..., are used in the calculations. The ΔE_{hyd} is corrected with the ZPV energy, and the ΔG_{hyd} is calculated at the room

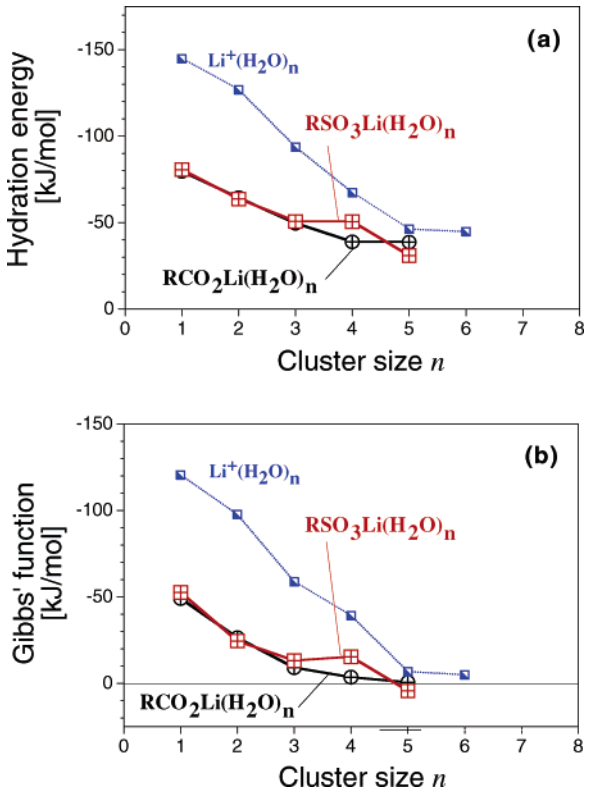

Figure 4. Size dependence of (a) the hydration energy ΔE_{hyd} with the ZPV energy correction and (b) the Gibbs function ΔG_{hyd} at room temperature for the perfluorinated lithium salt membranes evaluated with the 6-31+G* basis set on all the atoms and with the short-chain model. The units are given as kJ/mol. Gibbs' function ΔG_{hyd} is evaluated under the assumption of the ideal gas. The ΔE_{hyd} and ΔG_{hyd} of $Li^+(H_2O)_n$ with the same approximation level (refs 20 and 21) is also shown for comparison.

TABLE 3: Hydration Energy (ΔE_{Iso}) Summed into the ZPV Energy Correction and Gibbs' Function (ΔG_{Hyd}) of the Cluster-Modeled Perfluorinated Lithium Sulfonate and Carboxylate Membranes, $RSO_3Li(H_2O)_n$ and $RCO_2Li(H_2O)_n$

		short-chain				long-chain	
		basis (a)		HF/6-31+G*			
	n	ΔE_{hyd}	ΔG_{hyd}	ΔE_{hyd}	ΔG_{hyd}	ΔE_{hyd}	ΔG_{hyd}
$RSO_3Li(H_2O)_n$	1	−69.25	−42.39	−80.69	−52.65	−85.44	−54.40
	2	−71.01	−29.12	−63.66	−24.60	−64.19	−29.69
	3	−48.25	−13.85	−50.70	−13.28	−50.33	−9.90
	4	−51.55	−13.98	−50.66	−15.39		
	5	−26.73	5.36	−30.98	4.27		
$RCO_2Li(H_2O)_n$	1	−81.99	−51.36	−79.62	−49.13	−72.44	−43.38
	2	−63.82	−28.32	−64.30	−26.34	−67.07	−29.37
	3	−51.90	−12.80	−49.70	−9.15	−47.32	−7.17
	4	−39.76	−3.90	−38.84	−3.64		
	5	−41.98	−1.92	−38.67	−0.60		

[a] ΔG_{hyd} is evaluated at room temperature (298.15 K) under the assumption of the ideal gas. Data are expressed as kJ/mol. We show the cases of the basis set (a) and 6-31+G* level of the short-chain model and the long-chain model.

temperature (298.15 K) under the assumption of the ideal gas. The calculation level is HF/6-31+G* and the short-chain model is used.

Their numerical data are summarized in Table 3. We show the cases of the basis set (a) and the HF/6-31+G* level for the short-chain model. Although some influence can be seen for $n = 1$ and $n = 2$ of $RSO_3Li(H_2O)_n$, neither the ΔE_{hyd} nor the ΔG_{hyd} values are significantly influenced by the basis set or by the cluster model used. Therefore, it is sufficient to calculate the hydration energy with the small basis set (a). The perfluorinated chain exerts some slight influence on the ΔE_{hyd} and ΔG_{hyd}, because the hydration is dominantly determined by the hydrogen bond between the H_2O molecules or between the H_2O molecule and the functional group.

Up to $n = 3$, the two membrane systems, $RSO_3Li(H_2O)_n$ and $RCO_2Li(H_2O)_n$, have almost equal values for ΔE_{hyd} and ΔG_{hyd}. For $n = 4$, the $RSO_3Li(H_2O)_n$ system gives a larger ΔE_{hyd} and ΔG_{hyd} than the $RCO_2Li(H_2O)_n$ system. This can be explained by the difference in the number of hydrogen bonds. All the H_2O molecules are bound with hydrogen bonds(s) in the $RSO_3Li(H_2O)_n$ cluster, while the cluster $RCO_2Li(H_2O)_4$ is not so stabilized by the hydration due to the presence of free H_2O molecules in the cluster **4-a**.

For comparison, we have also drawn the size dependences of ΔE_{hyd} and ΔG_{hyd} of the hydrated lithium cation $Li^+(H_2O)_n$ up to $n = 6$[19−23] in Figure 4, given as follows;

$$Li^+(H_2O)_{n-1} + H_2O \rightarrow Li^+(H_2O)_n \qquad (6)$$

In the most stable structures of $Li^+(H_2O)_n$, a second hydration shell is constructed with the hydrogen bonds for $n \geq 5$, and the hydration number n dependences of the ΔE_{hyd} and ΔG_{hyd} then become very slight. Because the $Li^+(H_2O)_n$ cluster is a singly charged system, ΔE_{hyd} and ΔG_{hyd} of $Li^+(H_2O)_n$ are much larger than those of the perfluorinated Li salt membrane systems for the small hydration number n, whereas the hydrogen bond between the H_2O molecules provides a dominant contribution for the larger hydration number n, and the ΔE_{hyd} and ΔG_{hyd} of $RSO_3Li(H_2O)_n$ and $RCO_2Li(H_2O)_n$ show values close to those of $Li^+(H_2O)_n$.

The Gibbs' functions (ΔG_{hyd}) of both $RSO_3Li(H_2O)_n$ and $RCO_2Li(H_2O)_n$ are assumed to converge at about 0 kJ/mol for larger sizes of n (see Figure 4 and Table 3). Thus, after achieving the equilibrium condition, it is expected that the water molecules within the first shell will still remain, whereas almost all of the water molecules within the external shell will have evaporated away.

3.4. Estimation for the Evaporation of the Water Molecules. Since the observations of the IR spectra are carried out during the dehydration process and since the systems do not reach the equilibrium state, we estimated the evaporation ratio of the H_2O molecules within the ion cores. Suppose that the H_2O molecule evaporates when the kinetic energy is greater than the binding energy E_0 under the assumption of Maxwell−Boltzmann distribution, then the time t dependence of the concentration of water $c(t)$ within the ion core can be shown as the simplest first-order reaction:

$$c(t) = c_0 e^{-P(E_0)(t-t_0)} \qquad (7)$$

where c_0 is the initial concentration of H_2O at the initial time t_0, and the ratio of the H_2O molecule with a kinetic energy of more than E_0 is denoted as $P(E_0)$.

Figure 5 shows the E_0 vs the evaporation ratio of the H_2O molecules $1 - c(t)c_0$ surrounding the Li salt. The dehydration process in the experiment is continued for 24 h at room temperature, and then $T = 300$ K is assumed. The binding energy E_0 of the first hydration shell is regarded as more than 50 kJ/mol in both of the perfluorinated Li salt membrane systems (see ΔE_{hyd} in Figure 4 and Table 3), and almost none of the H_2O molecules evaporates during the 24 h of the dehydration process. If the E_0 is about 40 kJ/mol, then the evaporation ratio of the H_2O molecule $1 - c(t)/c_0$ is only 4%. In contrast, when the energy ΔE_{hyd} is 30 kJ/mol, the evaporation ratio $1 - c(t)/c_0$ is greater than 80%.

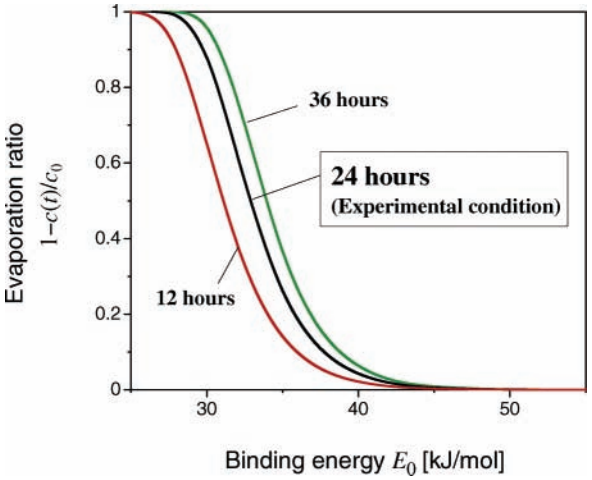

Figure 5. Evaporation ratio $1 - c(t)/c_0$ defined by eq 6 vs the binding energy of the H_2O molecule E_0 [kJ/mol]. The H_2O molecules in the ion parts are assumed to follow the Maxwell−Boltzmann distribution and the H_2O molecules with more than E_0 evaporate. The temperature T is assumed to be 300 K. Cases where the time of the dehydration process t is 12, 24, or 36 h are shown.

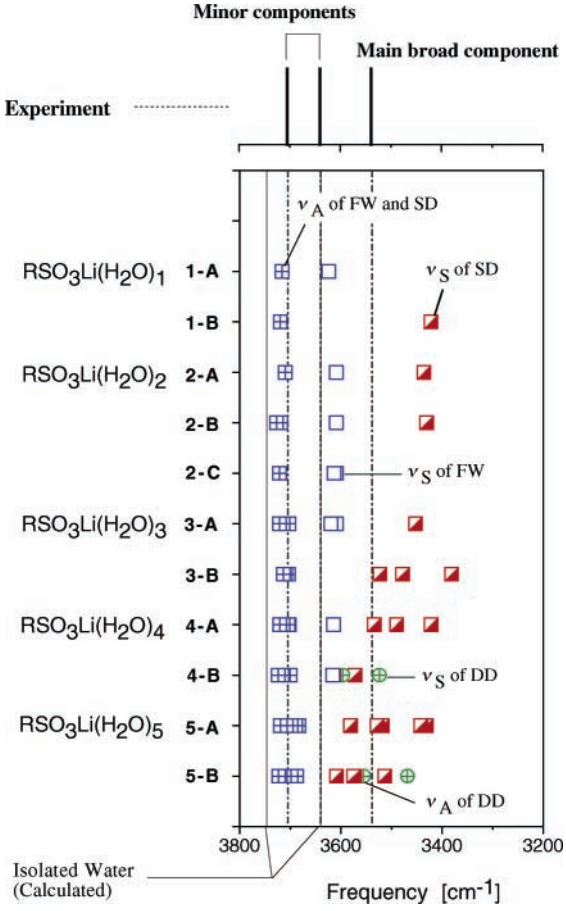

Figure 6. Calculated frequencies of the short-chain model $RSO_3Li(H_2O)_n$ ($R = HCF_2CF_2$) within the highest frequency region (more than 3200 cm^{-1}). The basis set used is the HF/6-31+G* on all the atoms. The clipped expressions SD, DD, and FW are single proton donor, double proton donor and free H_2O molecule, respectively. In the identification, the OH···F bond is treated as a free OH. The experimental frequencies are also shown with thick vertical broken lines and vertical bars in the upper part. The thin vertical solid lines (3746 and 3640 cm^{-1}) are the calculated frequencies of the free water molecules.

The binding energy E_0 of the external hydration shell can be estimated to be within the range of 30−40 kJ/mol by considering the size dependence of $\Delta E_{hyd}(n)$. We can therefore expect that the external hydration shell still remains within some of the ion cores but that the first shell is naked due to the evaporation of the external shell in several ion cores following the dehydration process.

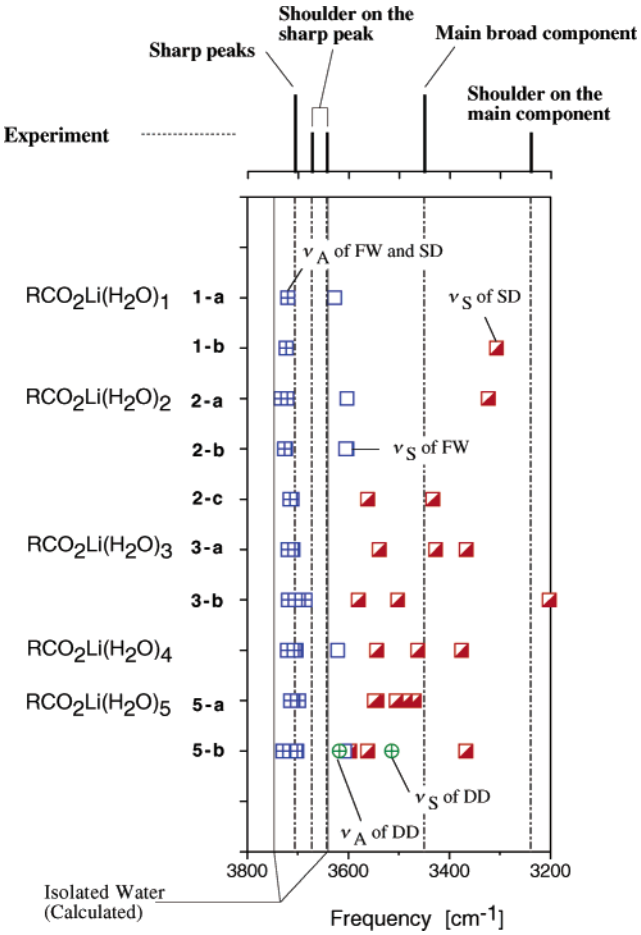

Figure 7. Calculated frequencies of the short-chain model $RCO_2Li(H_2O)_n$ ($R = HCF_2CF_2$) within the highest frequency region (more than 3200 cm^{-1}). The basis set used is the HF/6-31+G* on all the atoms. The clipped expressions SD, DD, and FW are single proton donor, double proton donor and free H_2O molecule, respectively. In the identification, the OH···F bond is treated as a free OH. The experimental frequencies are also shown with thick vertical broken lines and vertical bars in the upper part. The thin vertical solid lines (3746 and 3640 cm^{-1}) are the calculated frequencies of the free water molecules.

3.5. Calculated Normal Frequencies. 3.5.1. Calculated Frequency and the Water Molecule Type. Figures 6 and 7 show the calculated frequencies of the water molecule(s) in the perfluorinated Li sulfonate and carboxylate membranes $RSO_3Li(H_2O)_n$ and $RCO_2Li(H_2O)_n$ for the highest frequency region (more than 3200 cm^{-1}). Numerical data and more detailed identification are summarized in Tables 4 and 5. Since the basis set and the chain length do not influence the frequencies significantly, we show the normal frequencies for only the HF/6-31+G* level with the short-chain model.

The hydrogen bonds OH···OSO_2, OH···OCO, and OH···OH_2 play an important role in the character of the normal frequency of the H_2O molecule. Thus, the H_2O molecules can be classified into three types based on the number of hydrogen bonds. The H_2O molecules bound to one and two hydrogen bond(s) are denoted as "single proton donor" and "double proton donor", respectively. The H atom of the H_2O molecule is attracted by the SO_3 group, the CO_2 group or the neighboring H_2O molecule as a Lewis base molecule. The third type is "free H_2O molecule" which is bound to no Lewis base molecule with the hydrogen

TABLE 4: Calculated Frequencies for the Water Molecules Calculated with the Short-Chain Model $RSO_3Li(H_2O)_n$ (R = HCF″$_2$CF$_2$)[a]

		ν_A	ν_S	identification
		3750	3640	small peaks of the minor components
experiment			3539	broad peak of the main component
free H_2O (calcd)		3746	3640	
$RSO_3Li(H_2O)_1$	**1-A**	3716	3624	free
	1-B	3720	3422	OH···OSO_2
	1-C	3710	3436	OH···OSO_2
$RSO_3Li(H_2O)_2$	**2-A**	3728	3609	$H_2O(1)$ OH···F
		3719	3431	$H_2O(2)$ OH···OSO_2
	2-B	3721	3613	$H_2O(1)$ free
		3722	3609	$H_2O(2)$ free
$RSO_3Li(H_2O)_3$	**3-A**	3715	3620	$H_2O(1)$ OH···F
		3722	3609	$H_2O(2)$ free
		3703	3453	$H_2O(3)$ OH···OSO_2
	3-B	3704	3523	$H_2O(1)$ OH···OSO_2
		3714	3478	$H_2O(2)$ OH···OH_2
		3709	3381	$H_2O(3)$ OH···OSO_2
$RSO_3Li(H_2O)_4$	**4-A**	3714	3615	$H_2O(1)$ OH···F
		3705	3534	$H_2O(2)$ OH···OSO_2
		3702	3490	$H_2O(3)$ OH···OSO_2
		3721	3422	$H_2O(4)$ OH···OH_2
	4-B	3716	3616	$H_2O(1)$ OH···F
		3724	3596	$H_2O(2)$ OH···OH_2
		3701	3573	$H_2O(3)$ OH···OSO_2
		3596	3524	$H_2O(4)$ O_2SO···HOH···OH_2
$RSO_3Li(H_2O)_5$	**5-A**	3720	3581	$H_2O(1)$ OH···OH_2
		3708	3529	$H_2O(2)$ OH···OSO_2
		3690	3518	$H_2O(3)$ OH···OH_2
		3683	3442	$H_2O(4)$ OH···OSO_2
		3699	3432	$H_2O(5)$ OH···OH_2
	5-B	3723	3609	$H_2O(1)$ OH···OH_2
		3699	3575	$H_2O(2)$ OH···OSO_2
		3720	3573	$H_2O(3)$ OH···OH_2
		3688	3514	$H_2O(4)$ F···HOH···OH_2
		3555	3468	$H_2O(5)$ O_2SO···HOH···OH_2

[a] The basis set used is 6-31+G* on all of the atoms. The experimental frequencies are also summarized. The units used are cm^{-1}. The scaling factor 0.8941 is applied uniformly to enable a quantitative discussion. The identifications $H_2O(1)$, $H_2O(2)$, ..., correspond to the numbering in Figure 1.

TABLE 5: Calculated Frequencies for the Water Molecules Calculated with the Short-Chain Model $RCO_2Li(H_2O)_n$ (R = HCF″$_2$CF$_2$)[a]

		ν_A	ν_S	identification
experiment		3706		sharp peak of the minor component
		3672	3643	on the shoulder of the sharp peak
			3450	broad peak of the main component
			3240	on the shoulder of the broad peak
free H_2O (calcd)		3746	3640	
$RCO_2Li(H_2O)_1$	**1-a**	3720	3627	free
	1-b	3723	3303	OH···OCO
$RCO_2Li(H_2O)_2$	**2-a**	3733	3605	$H_2O(1)$ OH···F
		3722	3323	$H_2O(2)$ OH···OCO
	2-b	3726	3609	$H_2O(1)$ free
		3724	3603	$H_2O(2)$ free
	2-c	3715	3562	$H_2O(1)$ OH···OCO
		3711	3433	$H_2O(2)$ OH···OH_2
$RCO_2Li(H_2O)_3$	**3-a**	3719	3539	$H_2O(1)$ OH···OCO
		3712	3427	$H_2O(2)$ OH···OH_2
		3710	3367	$H_2O(3)$ OH···OCO
	3-b	3719	3580	$H_2O(1)$ OH···OH_2
		3705	3520	$H_2O(2)$ OH···OH_2
		3685	3202	$H_2O(3)$ OH···OCO
$RCO_2Li(H_2O)_4$		3720	3621	$H_2O(1)$ free
		3711	3544	$H_2O(2)$ OH···OCO
		3703	3463	$H_2O(3)$ OH···OH_2
		3706	3376	$H_2O(4)$ OH···OCO
$RCO_2Li(H_2O)_5$	**5-a**	3714	3649	$H_2O(1)$ OH···OCO
		3710	3549	$H_2O(2)$ OH···OH_2
		3711	3543	$H_2O(3)$ OH···OCO
		3709	3505	$H_2O(4)$ OH···OCO
		3698	3487	$H_2O(5)$ OH···OH_2
	5-b	3702	3607	$H_2O(1)$ free
		3729	3597	$H_2O(2)$ OH···OH_2
		3714	3562	$H_2O(3)$ OH···OCO
		3618	3514	$H_2O(4)$ H_2O···HOH···OH_2
		3705	3367	$H_2O(5)$ OH···OCO

[a] The basis set used is HF/6-31+G* on all of the atoms. The experimental frequencies are also summarized. The units used are in cm^{-1}. The scaling factor 0.8941 is applied uniformly to enable a quantitative discussion. The identifications $H_2O(1)$, $H_2O(2)$, ..., correspond to the numbering in Figure 2.

bond. As mentioned later, the H_2O molecule bound to the F atom is treated as the free H_2O molecule, because the F−H_2O hydrogen bond is very weak and the calculated normal frequency is almost the same as for the free H_2O molecule.

The frequencies of the asymmetric and symmetric stretching modes (denoted as ν_A and ν_S, respectively) of free H_2O molecules showed small red shifts from those of the isolated H_2O molecule. For example, the bands (3716 and 3624 cm^{-1}, respectively) in the isomer **1-A** and those (3720 and 3627 cm^{-1}, respectively) in the isomer **1-a** are a little smaller than those (3746 and 3640 cm^{-1}, respectively) of the isolated H_2O molecule.

In the single donor type, the calculated frequency of the asymmetric stretching mode (denoted as ν_A) shows a slight red shift from the isolated H_2O molecule. The red frequency shifts of ν_A from the isolated H_2O molecule (3746 cm^{-1}) are within only 70 cm^{-1} for all of the single donor H_2O molecules. In contrast, a markedly large red shift occurs in the frequency of the symmetric stretching mode (denoted as ν_S). The calculated frequencies of ν_S are 3431 and 3323 cm^{-1} in the $H_2O(2)$ of the isomers **2-A** and **2-a**, and their red shifts are 209 and 317 cm^{-1} from the ν_S of the isolated H_2O molecule (3640 cm^{-1}). The calculated frequencies of ν_S in the most stable isomers for $n \geq 3$ are distributed around 3500 cm^{-1}.

On the other hand, both the ν_A and ν_S show large red shifts from those of the isolated H_2O molecule in the double proton donor type. For example, the calculated frequencies of ν_A and ν_S are 3596 and 3524 cm^{-1} in $H_2O(4)$ of the isomer **4-B** and their degrees of red shift from the isolated H_2O molecule are 150 and 116 cm^{-1}, respectively.

Since the interaction between the H_2O and F atoms is very weak, the H_2O molecule with the OH···F bond does not show any significant red frequency shift. For example, the calculated ν_S is 3609 cm^{-1} for the $H_2O(1)$ in the isomer **2-A**, and its red frequency shift is only 31 cm^{-1}. The behavior of the frequency shift of H_2O molecule with the OH···F bond is the same as that of the free H_2O molecule. The hydrophobic feature of the F atoms is, therefore, appropriately described in terms of the normal frequencies.

3.5.2. Red Shift in the Frequency and Lewis Basicity. The red shift in the frequency is attributed to the fact that the OH bond of the H_2O molecule is weakened by the neighboring H_2O molecule or functional group that attracts the H atom of the OH bond by the formation of the hydrogen bond. Hence, the

TABLE 6: Calculated Natural Charges for the Water Molecules Calculated with the Short-Chain Model $RSO_3Li(H_2O)_n$ (R = HCF''_2CF_2)[a]

			H					
		O	free H atom		H-bonded		identification	
$RSO_3Li(H_2O)_1$	**1-A**	−1.042	0.533	0.533				free
	1-B	−1.098	0.528		0.565			$OH\cdots OSO_2$
	1-C	−1.085	0.524		0.561			$OH\cdots OSO_2$
$RSO_3Li(H_2O)_2$	**2-A**	−1.045	0.542	0.523			$H_2O(1)$	$OH\cdots F$
		−1.078	0.521		0.560		$H_2O(2)$	$OH\cdots OSO_2$
	2-B	−1.030	0.534	0.521			$H_2O(1)$	free
		−1.033	0.536	0.521			$H_2O(2)$	free
$RSO_3Li(H_2O)_3$	**3-A**	−1.026	0.530	0.519			$H_2O(1)$	$OH\cdots F$
		−1.026	0.534	0.517			$H_2O(2)$	free
		−1.059	0.514		0.553		$H_2O(3)$	$OH\cdots OSO_2$
	3-B	−1.067	0.518		0.554		$H_2O(1)$	$OH\cdots OSO_2$
		−1.079	0.516		0.561		$H_2O(2)$	$OH\cdots OH_2$
		−1.040	0.507		0.544		$H_2O(3)$	$OH\cdots OSO_2$
$RSO_3Li(H_2O)_4$	**4-A**	−1.021	0.529	0.515			$H_2O(1)$	$OH\cdots F$
		−1.037	0.504		0.541		$H_2O(2)$	$OH\cdots OSO_2$
		−1.052	0.511		0.545		$H_2O(3)$	$OH\cdots OSO_2$
		−1.065	0.512		0.557		$H_2O(4)$	$OH\cdots OH_2$
	4-B	−1.029	0.534	0.520			$H_2O(1)$	$OH\cdots F$
		−1.022	0.506		0.522		$H_2O(2)$	$OH\cdots OH_2$
		−1.041	0.520		0.543		$H_2O(3)$	$OH\cdots OSO_2$
		−1.074			0.542	0.539	$H_2O(4)$	$O_2SO\cdots HOH\cdots OH_2$
$RSO_3Li(H_2O)_5$	**5-A**	−1.032	0.507		0.531		$H_2O(1)$	$OH\cdots OH_2$
		−1.042	0.506		0.543		$H_2O(2)$	$OH\cdots OSO_2$
		−1.048	0.515		0.546		$H_2O(3)$	$OH\cdots OH_2$
		−1.064	0.519		0.554		$H_2O(4)$	$OH\cdots OSO_2$
		−1.061	0.513		0.554		$H_2O(5)$	$OH\cdots OH_2$
	5-B	−1.024	0.508		0.524		$H_2O(1)$	$OH\cdots OH_2$
		−1.041	0.521		0.543		$H_2O(2)$	$OH\cdots OSO_2$
		−1.035	0.507		0.534		$H_2O(3)$	$OH\cdots OH_2$
		−1.055	0.521		0.549		$H_2O(4)$	$F\cdots HOH\cdots OH_2$
		−1.093			0.551	0.547	$H_2O(5)$	$O_2SO\cdots HOH\cdots OH_2$

[a] The basis set used is HF/6-31+G* on all of the atoms. The identifications $H_2O(1)$, $H_2O(2)$, ..., correspond to the numbering in Figure 1.

degree of the red frequency shift is related to the Lewis basicity of the neighboring H_2O molecule or functional group, and mostly depends on the polarization of the H_2O molecule, especially in the ν_S of the single donor H_2O.

Tables 6 and 7 summarize the natural charges of the H_2O molecules in $RSO_3Li(H_2O)_n$ and $RCO_2Li(H_2O)_n$ with the short-chain model calculated at the 6-31+G* level. In the $H_2O(2)$ of **2-A**, $H_2O(3)$ of **3-A**, $H_2O(2)$ of **4-A**, and $H_2O(1)$ of **5-A**, their natural charges for O and hydrogen-bonded H atoms are (−1.078, +0.560), (−1.059, +0.553), (−1.037, +0.541), and (−1.032, +0.531), and their frequencies of ν_S are 3431, 3453, 3534, and 3581 cm^{-1}, respectively. The degree of the red shift of ν_S is well correlated with the strength of the polarization in these four H_2O molecules. In the figures and tables, we can see the tendency for a decrease in both the degree of the averaged red shift of ν_S and the strength of the polarization of the H_2O molecule, with the increment of the hydration number *n*.

In general, the frequency shift of the ν_S in the $RCO_2Li(H_2O)_n$ system is larger than the corresponding ν_S in the $RSO_3Li(H_2O)_n$ system, and this is consistent with the order of the strength of the acidity of their conjugate acids, RCO_2H and RSO_3H. For example, in the $H_2O(2)$ of **2-A** and the $H_2O(2)$ of **2-a**, their natural charges of O and H atoms are (−1.078, +0.560) and (−1.088, +0.559), respectively, and the frequencies of ν_S are 3431 and 3323 cm^{-1}.

3.6. Assignment of the Experimental IR Spectra. Experimentally observed IR spectra during the dehydration process are shown in the upper part of Figures 6 and 7 with thick vertical broken lines and vertical bars. The numerical data are summarized in Tables 4 and 5.

The small sharp peaks in the minor component at 3750 cm^{-1} for the $RSO_3Li(H_2O)_n$ systems in the observed IR spectra are easily assigned to the ν_A of the free H_2O molecule and the single proton donor, whereas the sharp peak at 3640 cm^{-1} of the $RSO_3Li(H_2O)_n$ is identified as the ν_S of the free H_2O molecule. This peak is found in the most stable isomers up to $n = 4$. Since the isomer **5-A** does not have a free H_2O molecule, there is no peak of ν_S in their calculated frequencies.

The broad band of the main component which has a peak at 3539 cm^{-1} in the $RSO_3Li(H_2O)_n$ system can be identified as the ν_S of the single proton donor H_2O molecule. For the larger size of *n*, there are many possible modes in the region at around 3500 cm^{-1}, and the overlapping of their contribution results in the formation of the broad peak. Because both ν_S and ν_A show a large low-frequency shift, the double proton donor H_2O molecule also contributes to form the broad band. We can assume that the double donor H_2O molecule exists commonly within the external hydration shell for the larger size of *n*.

The identification can be made for the $RCO_2Li(H_2O)_n$ system, similarly to that for the $RSO_3Li(H_2O)_n$ system. The sharp peak at 3706 cm^{-1} is identified as the ν_A of the free and single donor water molecules. One of the small peaks at 3643 cm^{-1} is assigned to the ν_S of the free H_2O molecule. The broad band at 3450 cm^{-1} is identified as the red-shifted ν_S with the attraction of the Lewis base, and it consists of the overlapping of the ν_S of the water molecules of the single proton donor in many isomers of varying sizes.

The IR spectra of the $RSO_3Li(H_2O)_n$ and the $RCO_2Li(H_2O)_n$ systems show the changing state of the H_2O molecules in the ion core during the dehydration process. At the initial stage of dehydration, single donors and double donors mainly exist

TABLE 7: Calculated Natural Charges for the Water Molecules Calculated with the Short-Chain Model $RCO_2Li(H_2O)_n$ (R = HCF''_2CF_2)[a]

			H					
		O	free H atom		H-bonded		identification	
$RCO_2Li(H_2O)_1$	**1-a**	−1.039	0.531	0.531				free
	1-b	−1.107	0.525		0.563			OH···OCO
$RCO_2Li(H_2O)_2$	**2-a**	−1.046	0.523	0.543			$H_2O(1)$	OH···F
		−1.088	0.518		0.559		$H_2O(2)$	OH···OCO
	2-b	−1.033	0.518	0.537			$H_2O(1)$	free
		−1.033	0.518	0.537			$H_2O(2)$	free
	2-c	−1.040	0.509		0.544		$H_2O(1)$	OH···OCO
		−1.079	0.521		0.560		$H_2O(2)$	$OH···OH_2$
$RCO_2Li(H_2O)_3$	**3-a**	−1.080	0.517		0.556		$H_2O(1)$	OH···OCO
		−1.071	0.517		0.558		$H_2O(2)$	$OH···OH_2$
		−1.042	0.508		0.544		$H_2O(3)$	OH···OCO
	3-b	−1.035	0.510		0.532		$H_2O(1)$	$OH···OH_2$
		−1.063	0.520		0.552		$H_2O(2)$	$OH···OH_2$
		−1.095	0.517		0.561		$H_2O(3)$	OH···OCO
$RCO_2Li(H_2O)_4$		−1.017	0.523	0.517			$H_2O(1)$	free
		−1.068	0.511		0.550		$H_2O(2)$	OH···OCO
		−1.041	0.507		0.541		$H_2O(3)$	$OH···OH_2$
		−1.053	0.511		0.551		$H_2O(4)$	OH···OCO
$RCO_2Li(H_2O)_5$	**5-a**	−1.037	0.505		0.537		$H_2O(1)$	OH···OCO
		−1.039	0.506		0.541		$H_2O(2)$	$OH···OH_2$
		−1.053	0.511		0.550		$H_2O(3)$	OH···OCO
		−1.042	0.509		0.539		$H_2O(4)$	OH···OCO
		−1.048	0.509		0.549		$H_2O(5)$	$OH···OH_2$
	5-b	−1.032	0.531		0.524		$H_2O(1)$	free
		−1.024	0.504		0.524		$H_2O(2)$	$OH···OH_2$
		−1.038	0.504		0.537		$H_2O(3)$	OH···OCO
		−1.075			0.538	0.544	$H_2O(4)$	$H_2O···HOH···OH_2$
		−1.072	0.514		0.552		$H_2O(5)$	OH···OCO

[a] The basis set used is HF/6-31+G* on all of the atoms. The identifications $H_2O(1)$, $H_2O(2)$, ..., correspond to the numbering in Figure 2.

within the external shell and they contribute to the observed IR spectra, whereas the free H_2O molecule within the first shell and the single donor H_2O molecule provide a significant contribution at the final stage of dehydration.

The peaks assigned to the free H_2O molecule are characteristic in the clusters that have a small hydration number. The contribution of the free H_2O molecule is assumed to be small for the larger hydration number *n*, because the external shell constructs the hydrogen bond network and almost all the H_2O molecules are bound to another H_2O molecule. Consequently, we can assume that some of the Li ion core still has the external hydration shell, but that there are several ion cores in which the external hydration shell has evaporated away, leaving only a few remaining hydrated molecules, including some free H_2O molecules, after the dehydration processes.

Within the IR spectra of the $RCO_2Li(H_2O)_n$ system, however, there are two small peaks at 3672 and 3240 cm^{-1} in addition to the currently mentioned peaks. One possible hypothesis is that they could be assigned to the ν_S and ν_A of $H_2O(3)$ of the isomer **3-b**, whose calculated frequencies are 3685 and 3202 cm^{-1}. They show a particularly red shift compared to the other water molecules due to the strong Lewis basicity of the CO_2 group. The isomer **3-b** is not the most stable structure, however the observations are carried out not after reaching an equilibrium but during the actual evaporation process, and it may be possible that they were trapped into such a metastable state.

3.7. IR Intensities. The calculated IR intensities of ν_A and ν_S are 100−200 and 20−100 km/mol, respectively, in the free H_2O molecule. Because the motions are localized on the appropriate H_2O molecule, the ratio of these intensities of the free H_2O molecule is qualitatively equal to that of the isolated H_2O molecule.

The intensity of ν_A for the single donor is 100−200 km/mol and is equal to that for the free H_2O molecule. Because the dominant contribution to the vibration is given by the stretching of the OH bond without forming the hydrogen bond, its motion is also localized on the appropriate H_2O molecule. In contrast, the intensity of ν_S for the single donor is 200−1000 km/mol. Because the stretching of the OH bond with the hydrogen bond contributes dominantly in the vibration mode due to the delocalization of the motion to the adjacent H_2O molecules, the variation of the dipole moment with the vibration becomes large in ν_S for the single donor.

In the double proton donor, the intensities of ν_A and ν_S are 300−400 and 200−1000 km/mol, respectively. Since two OH bonds form the hydrogen bond, the modes of both ν_A and ν_S are delocalized to the adjacent H_2O molecules. In terms of the IR intensity, we can understand that the contributions of ν_S of the single donor and both stretching modes of the double donor are significant in the broad peak of the main component observed with the experiment.

Because a large variation in the dipole moment is expected in the strongly polarized H_2O molecule, the IR intensity also shows a positive correlation with the red frequency shift, especially in ν_S. For example, in $H_2O(3)$ for the isomer **3-b**, the frequency of ν_S is strongly red shifted at 3202 cm^{-1} and the IR intensity becomes 1070 km/mol with the short-chain model at the HF/6-31+G* level.

3.8. Simple Analysis of the Characteristic Frequency Shift of Water Molecules. The remaining problems are the mode dependence of the degree of the frequency shift and the difference between single and double proton donor cases. The fact that only ν_S shows a large red shift while ν_A shows a slight shift in the single proton donor, whereas both ν_S and ν_A show a large frequency shift in the double proton donor, can be understood with an analysis of the classical coupled oscillator system. If we suppose that the water molecule is the coupled

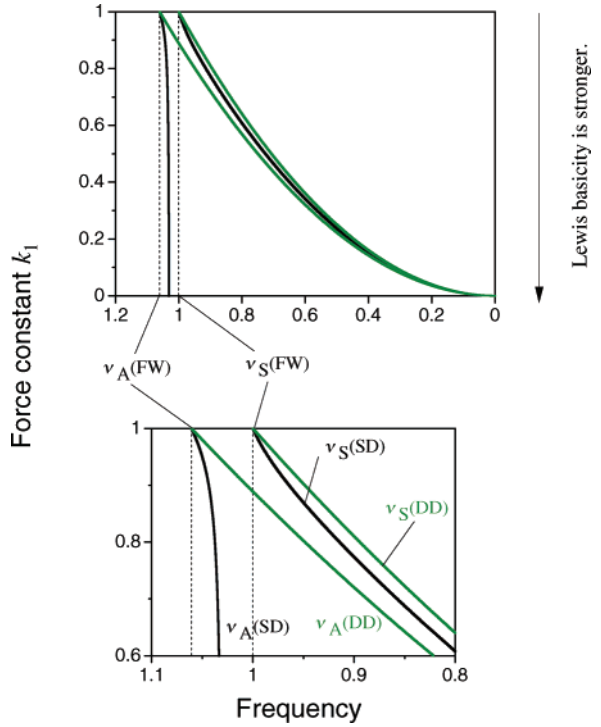

Figure 8. Frequencies ν_A and ν_S vs the force constant calculated with the classical coupled oscillator systems given in eqs 8 and 9. Here, $m_O = 16$, $m_H = 1$, and the force constant of OH of the free water molecule (without attraction by the Lewis base) is normalized to 1. The clipped expressions SD, DD, and FW are single proton donor, double proton donor and free H_2O molecule, respectively. In the SD, the value of k_2 is kept a constant (one of the OH bonds is bound to no Lewis base molecule), and the assumption of $k_1 = k_2$ is used in the DD (the same Lewis base is bound to both OH bonds).

oscillator system, then the frequencies of ν_A and ν_S are given as follows:

$$\nu_A^2 = \frac{k_1 + k_2}{2} \times \frac{m_O + m_H}{m_O m_H} \frac{1}{2} \sqrt{(k_1 - k_2)^2 \cdot \frac{m_O + m_H}{m_O m_H} + \frac{(k_1 + k_2)^2}{m_O^2}} \quad (8)$$

and

$$\nu_S^2 = \frac{k_1 + k_2}{2} \times \frac{m_O + m_H}{m_O m_H^2} \frac{1}{2} \sqrt{(k_1 - k_2)^2 \cdot \frac{m_O + m_H}{m_O m_H^2} + \frac{(k_1 + k_2)^2}{m_O^2}} \quad (9)$$

where m_O and m_H are the masses of the oxygen and hydrogen atoms, respectively. The force constants of two OH bonds within the H_2O molecule are k_1 and k_2. The frequencies of the asymmetric and symmetric stretching modes of the free H_2O molecule become $\nu_A(\mathrm{FW}) = k_1 (m_O + 2m_H)/m_O m_H$ and $\nu_S(\mathrm{FW}) = k_1/m_H$. The attraction of the Lewis base can be expressed by a reduction in the force constants k_1 and k_2.

Figure 8 shows the k_1 dependence of the frequencies ν_A and ν_S given by eqs 8 and 9. The masses m_O and m_H are assumed to be 16 and 1, and the k_1 and k_2 of the free H_2O molecule are normalized to 1. The figure clearly shows the Lewis basicity dependence of the low-frequency shift mentioned in the present work for the two frequencies ν_A and ν_S in both the single and the double proton donors.

Because it is attributed to the Lewis basicity, the same characteristic frequency shift is generally seen in systems involving H_2O molecules. It is also seen in the IR spectra of the H_2O molecule combined with the organic base molecule(s) in the CCl_4 solution,[24] and moreover, the same frequency shift is observed in the cluster of the gaseous phase, such as $C_6H_5OH(H_2O)_n$.[25−26]

4. Conclusion

Using an ab initio MO method, the normal frequencies have been calculated for the perfluorinated Li sulfonate and carboxylate membranes through means of cluster models, in an effort to analyze their infrared (IR) spectra which are observed experimentally during the dehydration process. The normal frequency of the water molecule shows the typical shift of the hydrogen bond system. The dominant component with a broad peak at about 3500 cm^{-1} is identified as the H_2O molecule combined with the external hydration shell, while the small sharp peaks at about 3750 cm^{-1} are identified as the ν_A of the single donor and the free H_2O molecules. The sharp peak at about 3650 cm^{-1} also shows that free H_2O molecules are also found in the cluster with small hydration number of n.

The evaporation ratio $1 - c(t)/c_0$ shows that the H_2O molecules within the external hydration shells of several ion cores are able to evaporate during the dehydration process, but it is difficult for the H_2O molecules within the first shell to evaporate under the experimental conditions. In the observed IR spectra, there is only the main component of the broad adsorption band before dehydration, and the sharp peaks as minor components appear at the shoulder of the broad band during 24 h of dehydration. Hence, it can be concluded that the H_2O molecules of the external hydration shell still remain in several ion cores, but that the external shell has evaporated, and that the first hydration shells continue to be naked in some of the other ion cores following the dehydration process.

Acknowledgment. The authors gratefully thank Dr. R. Iwamoto for presenting valuable experimental data and providing helpful discussions.

References and Notes

(1) Robertson, M. A. F.; Yeager, H. L. In *Ionomers-Synthesis, Structure, Properties and Applications*; Tant, M. R., Mauritz, K. A., Wilkes, G. L., Eds.; Chapman & Hall: London, 1997; pp 290−330 and references therein.

(2) Fujimura, M.; Hashimoto, T.; Kawai, H. *Macromolecules* **1981**, *14*, 1309.

(3) Fujimura, M.; Hashimoto, T.; Kawai, H. *Macromolecules* **1982**, *15*, 136.

(4) Yeager, H. L.; Gronowski, A. A. In *Ionomers-Synthesis, Structure, Properties and Applications*; Tant, M. R., Mauritz, K. A., Wilkes, G. L., Eds.; Chapman & Hall: London, 1997; pp 333−364.

(5) Falk, M. *Can. J. Chem.* **1980**, *58*, 1495.

(6) Lowry, S. R.; Mauritz, K. A. *J. Am. Chem. Soc.* **1980**, *102*, 4665.

(7) Lopez, M.; Kipling, B.; Yeager, H. L. *Anal. Chem.* **1976**, *48*, 1120.

(8) Ostrowska, J.; Narebska, A. *Colloid Polym. Sci.* **1983**, *261*, 93.

(9) Bunce, N. J.; Sondheimer, S. J.; Fyfe, C. A. *Macromolecules* **1986**, *19*, 333.

(10) Sondheimer, S. J.; Bunge, N. J.; Lemke, M. E.; Fyfe, C. A. *Macromolecules* **1986**, *19*, 339.

(11) MacMillan, B.; Sharp, A. R.; Armstrong, R. L. *Polymer* **1999**, *40*, 2471.

(12) Lee, E. M.; Thomas, R. K.; Burgess, A. N.; Barnes, D. J.; Soper, A. K.; Rennie, A. R. *Macromolecules* **1992**, *25*, 3106.

(13) Sodaye, H. S.; Pyjari, P. K.; Goswami, A.; Manohar, S. B. *J. Polym. Sci., Part B: Polym. Phys.* **1997**, *35*, 771.

(14) Sodaye, H. S.; Pyjari, P. K.; Goswami, A.; Manohar, S. B. *J. Polym. Sci., Part B: Polym. Phys.*, **1998**, *36*, 983.

(15) Kuptsov, A. H.; Zhinzhin, G. N. *Handbook of Fourier Transform Raman and Infrared Spectra of Polymers*; Elsevier: Amsterdam, 1988; p 44.
(16) Iwamoto, R.; Oguro, K.; Sato, M.; Iseki, Y. *J. Phys. Chem. B*, **2002**, *106*, 6973.
(17) Private communication to R. Iwamoto.
(18) Gaussian 98, Revision A.9, Frisch, M. J.; Trucks, G. W.; Schlegel, H. B.; Scuseria, G. E.; Robb, M. A.; Cheeseman, J. R.; Zakrzewski, V. G.; Montgomery, J. A., Jr.; Stratmann, R. E.; Burant, J. C.; Dapprich, S.; Millam, J. M.; Daniels, A. D.; Kudin, K. N.; Strain, M. C.; Farkas, O.; Tomasi, J.; Barone, V.; Cossi, M.; Cammi, R.; Mennucci, B.; Pomelli, C.; Adamo, C.; Clifford, S.; Ochterski, J.; Petersson, G. A.; Ayala, P. Y.; Cui, Q.; Morokuma, K.; Malick, D. K.; Rabuck, A. D.; Raghavachari, K.; Foresman, J. B,; Cioslowski, J.; Ortiz, J. V.; Baboul, A. G.; Stefanov, B. B.; Liu, G.; Liashenko, A.; Piskorz, P.; Komaromi, I.; Gomperts, R.; Martin, R. L.; Fox, T. D.; Keith, J.; Al-Laham, M. A.; Peng, C. Y.; Nanayakkara, A.; Challacombe, M.; Gill, P. M. W.; Johnson, B.; Chen, W.; Wong, M. W.; Andres, J. L.; Gonzalez, C.; Head-Gordon, M.; Replogle, E. S.; Pople, J. A.; Gaussian, Inc.: Pittsburgh, PA, 1998.
(19) Yamaji, K.; Makita, Y.; Watanabe, H.; Sonoda, A.; Kanoh, H.; Hirotsu, T.; Ooi, K. *J. Phys. Chem. A* **2001**, *105*, 602.
(20) Watanabe, H.; Yamaji, K.; Sonoda, A.; Makita, Y.; Kanoh, H.; Ooi, K. *J. Phys. Chem. A* **2003**, *107*, 7832.
(21) Yanase, S.; Oi, T. *J. Nucl. Sci. Technol.* **2002**, *39*, 1060.
(22) Pye, C. C. *Int. J. Quantum Chem.* **2000**, *76*, 62.
(23) Pye, C. C.; Poirier, R. A.; Rudolph, W. *J. Phys. Chem.* **1996**, *100*, 601.
(24) Schiöberg, D.; Luck, W. A. P. *J. Chem. Soc., Faraday Trans.* **1979**, *75*, 762.
(25) Watanabe, H.; Iwata, S. *J. Phys. Chem.* **1996**, *105*, 420.
(26) Watanabe, T.; Ebata, T.; Tanabe, S.; Mikami, N. *J. Phys. Chem.* **1996**, *105*, 408.